Binding Kinetics of Harmonically Confined Random Walkers

Sebastian Sensale[‡*], Pranav Sharma[‡], and Gaurav Arya[‡*]
[‡]*Department of Mechanical Engineering and Materials Science, Duke University, Durham, NC 27708, USA*
(Dated: March 31, 2022)

Diffusion-mediated binding of molecules under the influence of discrete spatially confining potentials is a commonly encountered scenario in systems subjected to explicit fields or implicit fields arising from tethering restraints. Here, we derive analytical expressions for the mean binding time of two random walkers geometrically confined by means of two harmonic potentials in one and two dimensional systems, which show excellent agreement with Brownian dynamics simulations. As demonstration of its utility, we use this theory to maximize the communication speed in existing DNA walkers, obtaining quantitative agreement with previously reported experimental findings. The analytical expressions derived in this work are broadly applicable to diverse systems, providing new ways to characterize communication processes and optimize the rate of signal propagation for sensing and computing applications at the nanoscale.

I. INTRODUCTION

Diffusion-mediated molecular binding events play a central role in biology, catalysis, molecular sensing, medical diagnostics, and nanotechnology [1, 2]. A commonly encountered scenario is that of a freely diffusing particle binding to a fixed target, and the problem of predicting its associated binding time has attracted much theoretical interest [3]. Due to the stochastic nature of both diffusion and binding, a probabilistic approach is required to characterize binding times, usually in terms of their distribution and mean. This typically entails deriving a differential equation governing the "survival" probability of the particle [1], and solving the resulting equation in the diffusion domain $\Omega \subset \mathbb{R}^d$ with appropriate boundary conditions that reflect the geometry and nature (absorbing, partly absorbing, or reflecting) of the boundary and the target. Such formalism has been applied to a wide spectrum of problems, ranging from basic ones involving geometrically simple domains whose entire boundaries serve as targets [4, 5], to more complex ones involving: small targets on the domain boundary (narrow-escape problem [6]); multiple targets on a surface [7]; infinite periodic lattices of particles and targets [8]; non-convex domain geometries such as networks and fractals [9]; anomalous diffusion due to crowding or viscoelastic effects [10]; coupled diffusive processes in multiple dimensions [11]; and external biasing potentials [12].

There exists another binding scenario—that of diffusing particles binding to each other instead of to fixed targets—which has received far less attention [13]. The first attempt at solving the binding rate for this bimolecular scenario can be traced back to the works of Smoluchowski [14], who reduced a system of two species of freely diffusing particles in an infinite domain into an effective one-walker scenario, wherein a single walker (representing the distance between the two original walkers) diffuses towards a fixed target. In the presence of domain boundaries, the additional length and timescales associated with particle collisions with the boundaries generally make unsuitable such approaches used to estimate binding rates for free diffusion [13, 15]. However, when the explicit physical confinement is replaced by a more implicit confinement due to the action of an external optical, electric, or magnetic field [16], or due to soft physical attachment of the particle (for instance, via polymer tethers [17]), some of these approaches may still be salvaged [18]. While advances in modeling binding under such confinement have been made [19], no explicit expressions for the mean binding time of two particles diffusing in independent harmonic potentials have been reported to this date. In this work, such expressions are derived for one and two dimensional systems by combining the approach proposed by Smoluchowski to reduce the dimensionality of the system with a first passage time approach introduced by Szabo *et al.* [20]. These expressions are compared against discrete-space and continuous-time Brownian dynamics simulations [21], showing excellent agreement. To show how these expressions can be used to study real-life molecular binding processes, explicit estimates for the mean binding time of a system of communicating DNA walkers introduced by Li *et al.* [22] are derived, providing theoretical insight into how to enhance signal propagation and revealing a reaction-limited upper bound for the communication speed of this nanotechnology only suggested experimentally heretofore. While we use binding of DNA walkers as one illustration of the usefulness of our proposed theory, the scope of our theory extends much further than this example. The spread of infections in animal motion from home ranges [19], the kinetics of V-DJ recombination in chromatin [23], the modulation of protein-ligand activity through tethering of binding agents [24], and molecular detection through tethered particle sandwich assays [25], all these processes involve the binding of partners diffusing within confining potentials, and their dynamics could be treated using the formalism introduced in this article.

II. ANALYTICAL MODEL

A. Derivation in one dimension

Consider two identical random walkers of diffusion coefficient D moving in one dimension ($d = 1$) around attractive centers located at $x_0 = 0$ and $x_0' = a$ (≥ 0), respectively. By modeling the attraction to these centers through identical harmonic potentials with second derivative k, the joint probability of finding the particles at positions x and x' is given by

$$P(x, x') = \left(\frac{\beta k}{2\pi}\right) e^{-\frac{\beta k}{2}(x^2 + (x'-a)^2)}, \tag{1}$$

where $\beta = 1/k_B T$ is the reciprocal of the thermal energy. Writing $x' = x + r$, integrating the probability over all values of x, and normalizing the result for $r \in [\epsilon, +\infty]$, where ϵ is the distance at which the walkers bind (or react), the probability density for a distance r between the walkers is given by

$$Q(r) = \sqrt{\frac{\beta k}{\pi}} \left(\frac{e^{-\frac{\beta k}{4}(a-r)^2}}{\mathrm{erfc}\left(\frac{\sqrt{\beta k}}{2}(\epsilon - a)\right)} \right), \tag{2}$$

where erfc is the complementary error function. This probability density is displayed in Fig. 1 for different separations a of the attracting centers. As the particles prefer to be located at the centers of their respective harmonic wells, a maximum is found at $r = a$.

We note that the effect of this bias on the binding dynamics of two walkers is similar to that of an external potential $U(r) = -\frac{1}{\beta}\ln[Q(r)]$ on the dynamics of a single one-dimensional walker moving as the distance between the two walkers $r \in [\epsilon, +\infty]$. The problem of finding the mean binding time τ of the two walkers then becomes equivalent to that of determining the mean first passage time (MFPT) of a one-dimensional walker through a partially absorbing wall at $r = \epsilon$. Since this external potential is confining to the walker ($\beta U \to +\infty$ as $r \gg a$), the MFPT is expected to be finite. Assuming Boltzmann-distributed initial positions of the walker, the MFPT through the wall is given by [20]

$$\tau = \frac{1}{2D} \int_{\epsilon}^{+\infty} \frac{dr}{Q(r)} \left[\int_{r}^{+\infty} Q(y) dy \right]^2 + \frac{1}{\kappa Q(\epsilon)}, \tag{3}$$

where a diffusion coefficient of $2D$ is imposed, as our new walker exhibits a mean square displacement in coordinate r that is twice that of the original walkers in coordinates x and x' [1]. The parameter κ (in units of length per time) accounts for the reactivity of the wall: when $\kappa \to \infty$ the walkers bind instantly upon first contact, while for $\kappa = 0$ the walkers are reflected back at every encounter [26, 27].

Decomposing the MFPT obtained from Eqs. 2 and 3 as $\tau = \tau_D + \tau_\kappa$, where the first term represents the MFPT to a fully absorbing wall and the second term accounts for reflections on a partially absorbing one, and normalizing all lengths and times by $1/\sqrt{\beta k}$ and $1/2D\beta k$, we find

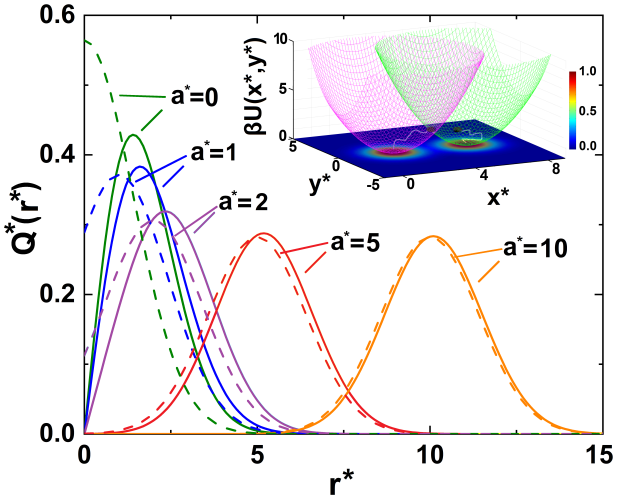

FIG. 1. Probability density $Q(r)$ of observing two random walkers a distance r apart in $d = 1$ (dashed lines) and $d = 2$ (solid lines) for $\epsilon = 0$. For $d = 2$, $Q \to 0$ as $r \to 0$ due to vanishing entropy (Jacobian factor) with r in dimensions higher than one. Inset: Illustration of two walkers in 2D diffusing in distinct harmonic wells whose centers are a distance $a = 4$ apart. In all plots βk is set equal to 1.

$$\tau_D^* = \frac{\sqrt{\pi}}{\mathrm{erfc}(-\alpha^*/2)} \int_{-\alpha^*}^{+\infty} [\mathrm{erfc}(\xi/2)]^2 \, e^{(\xi/2)^2} d\xi, \tag{4a}$$

$$\tau_\kappa^* = \lambda^* \sqrt{\pi} \, \mathrm{erfc}(-\alpha^*/2) e^{(\alpha^*/2)^2}, \tag{4b}$$

where $a^* \equiv \sqrt{\beta k} a$, $\epsilon^* \equiv \sqrt{\beta k}\epsilon$, $\tau_D^* \equiv 2D\beta k \tau_D$, $\tau_\kappa^* \equiv 2D\beta k \tau_\kappa$, $\lambda^* \equiv 2D\sqrt{\beta k}/\kappa$, and $\alpha^* \equiv a^* - \epsilon^*$. For small values of λ^*, binding is diffusion limited and the MFPT is determined merely by the first encounter time of the walkers τ_D^*. For moderate or large values of λ^*, the MFPT depends on the first encounter of the two walkers and all subsequent excursion times in the domain.

Figures 2a and 2b display τ_D^* and τ_κ^* as a function of ϵ^* for multiple values of a^*. As expected, both times decay with increasing binding distance ϵ of the walkers. Furthermore, because τ_D and τ_κ are functions of the difference in a and ϵ (Eqs. 4a and 4b), changes in a merely shift the binding time curve laterally in the ϵ direction without changing its shape. Interesting conclusions can also be drawn by analyzing the limiting behaviors of τ_D and τ_κ at $\alpha^* \approx 0$ (two walkers diffusing in the same potential) and $\alpha^* \gg 1$ (two walkers diffusing in potentials whose centers are far apart). Estimating the integral in Eq. 4a by its value from 0 to infinity for $\alpha^* \approx 0$ and using the imaginary error function for $\alpha^* \gg 1$, we obtain

$$\tau_D \approx \begin{cases} \frac{\ln 2}{D\beta k} & \text{for } \alpha^* \approx 0, \\ \frac{\pi}{D\beta k} \mathrm{erfi}\left(\frac{\sqrt{\beta k}}{2}(a - \epsilon)\right) & \text{for } \alpha^* \gg 1. \end{cases} \tag{5}$$

While the first encounter time decreases with the diffusion coefficient as D^{-1} (and so does the tail of the survival probability, which may be estimated by $S(t) \sim e^{-t/\tau}$ [20]), the behavior with respect to $\sqrt{\beta k}$ is non-monotonic: steep potentials expedite encounters for small separations and hinder them for larger ones (Fig. 2c). As τ_κ includes the dynamics of the walkers upon reflection, this behavior with $\sqrt{\beta k}$ is also observed for τ_κ, as shown in Fig. 2d. Detailed derivations of Eqs. 2–5 can be found in Sec. 1 of [28].

B. Derivation in two dimensions

The approach introduced above can be extended to the case of two random walkers (of diffusion coefficients D) moving in two dimensions ($d = 2$) within harmonic potentials (of second derivative k in both dimensions) centered at $\mathbf{r}_0 = (0, 0)$ and $\mathbf{r}'_0 = (a, 0)$, respectively. The joint probability of finding our particles at positions (x, y) and (x', y') is given by

$$P(x, y, x', y') = \left(\frac{\beta k}{2\pi}\right)^2 e^{-\beta\frac{k}{2}(x^2+y^2+(x'-a)^2+y'^2)}. \quad (6)$$

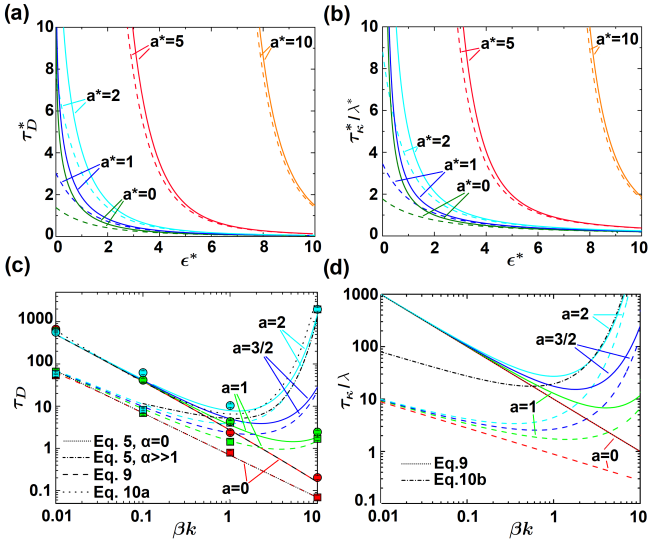

FIG. 2. Variation of the mean binding time with binding distance and steepness of potential: (a,b) Components τ_D^* and τ_κ^*/λ^* as a function of ϵ^* for $d = 1$ (dashed lines) and $d = 2$ (solid lines). (c,d) τ_D and $\tau_\kappa/\lambda = \tau_\kappa\kappa\sqrt{\beta k}$ as a function of βk for different values of a with $D = 1$ and $\kappa = 1$ (dashed lines for $d = 1$ and $\epsilon = 0$, solid lines for $d = 2$ and $\epsilon = 0.1$). All other lines (colored black) represent analytical asymptotes (large a^* approximations evaluated at $a = 2$, $X = 1$). In (c), squares (1D) and circles (2D) represent average MFPTs obtained from 100 Brownian simulations carried out for each set of parameters with $D = 1$ and a spatial mesh spacing of $\Delta = 1/20$, as described in Sec. 3 of [28]

.

Writing the position of the walker moving around a in a system of polar coordinates centered on the walker moving around the origin [$x' = x + r\cos(\theta)$ and $y' = y + r\sin(\theta)$] and integrating over all values of x, y, and θ, an effective orientationally averaged probability density devoid of any anisotropy is derived, which characterizes the probability density for observing a distance r between the walkers,

$$Q(r) = \frac{re^{-\frac{\beta k}{4}r^2} I_0\left(\beta kar/2\right)}{\int_\epsilon^{+\infty} re^{-\frac{\beta k}{4}r^2} I_0\left(\beta kar/2\right) dr}, \quad (7)$$

where I_0 is the modified Bessel function of the first kind and order zero (see Sec. 2.1 of [28] for a detailed derivation of Eq. 7). Fig. 1 shows $Q(r)$ for different values of a. Except for the zero intercept at $r = 0$, this density exhibits strong similarity with that of one-dimensional walkers. Substituting our radially symmetric distribution function (Eq. 7) in Eq. 3, normalizing all lengths by $1/\sqrt{\beta k}$, all times by $1/2D\beta k$, and decomposing the MFPT as $\tau^* = \tau_D^* + \tau_\kappa^*$, we obtain

$$\tau_D^* = \frac{\int_{\epsilon^*}^{+\infty} \frac{\left(\int_\xi^{+\infty} \eta \exp(-\eta^2/4) I_0(a^*\eta/2) d\eta\right)^2}{\xi \exp(-\xi^2/4) I_0(a^*\xi/2)} d\xi}{\int_{\epsilon^*}^{+\infty} \xi \exp(-\xi^2/4) I_0(a^*\xi/2) d\xi}, \quad (8a)$$

$$\tau_\kappa^* = \lambda^* \frac{\int_{\epsilon^*}^{+\infty} \xi \exp(-\xi^2/4) I_0(a^*\xi/2) d\xi}{\epsilon^* \exp(-\epsilon^{*2}/4) I_0(a^*\epsilon^*/2)}. \quad (8b)$$

The two components are plotted in Figs. 2a and 2b as a function of ϵ^* for multiple values of a^*. While these expressions were numerically determined, we will study a few limiting cases to uncover scalings of the mean binding time. In the limit of two walkers moving in the same interval ($a^* \to 0$), τ simplifies to

$$\tau = \frac{1}{D\beta k}\left(\int_\epsilon^{+\infty} \frac{e^{\frac{\beta k}{4}(\epsilon^2 - x^2)}}{x} dx + \frac{2D}{\kappa\epsilon}\right), \quad (9)$$

which decreases with increasing $\sqrt{\beta k}$, as in the $d = 1$ case. While collisions happen in finite times for any confined domain in one dimension, there is a vanishing probability of finding a point in dimensions higher than one [19], and thus τ blows up as $\epsilon \to 0$ for $d = 2$. For large a^* and small ϵ^*, the mean binding time scales as

$$\tau_D \approx \frac{1}{D\beta k}\left[e^{\frac{\beta k}{4}a^2} \ln\left(\frac{X}{\epsilon}\right) + \frac{2e^{-\frac{\beta k}{4}(X-a)^2}}{\sqrt{\pi a}(\beta k)^{\frac{3}{2}} X^{\frac{5}{2}}}\right], \quad (10a)$$

$$\tau_\kappa \approx \frac{2}{\kappa}\sqrt{\frac{\pi a}{\epsilon\beta k}} e^{\frac{\beta k}{4}(a-\epsilon)^2}, \quad (10b)$$

for a suitable value of X found to be between $1/\sqrt{\beta k}$ and $2/\sqrt{\beta k}$ that best approximates the behavior of Eq. 8a (see Sec. 2.2 of [28] for details). These expressions show that, for large values of a^*, τ rises sharply with increasing $\sqrt{\beta k}$ (also see Fig. 2c), as in the $d = 1$ case, and it blows up as $\epsilon \to 0$. This behavior with $\sqrt{\beta k}$ is also observed for τ_κ, as shown in Fig. 2d.

An underlying hypothesis here is that the MFPT derived from an ensemble-average of the MFPTs associated with Boltzmann-distributed initial positions of the two walkers in the original 4-dimensional potential energy surface can be approximated by the MFPT of an ensemble-averaged effective energy landscape describing the probability distribution of the distance between the walkers. This same hypothesis was considered by Bell and Terentjev [18] to characterize the rate of binding of a grafted polymer to a surface receptor. The accuracy of this hypothesis was tested by comparing our analytical MFPTs for the $d = 1$ and $d = 2$ scenarios against explicit overdamped Brownian dynamics simulations of random walkers in discrete space and continuous time using a recently proposed algorithm [21]. This comparison shown in Fig. 2c, and in Sec. 3 of [28], indicates excellent agreement between theory and simulations.

III. APPLICATION TO DNA NANOTECHNOLOGY

To demonstrate the utility of the model developed here, we apply it to quantify the communication speed of the "DNA acrobats" introduced by Li *et al.* [22], and make use of the non-monotonic behavior of τ seen in Figs. 2c and 2d to optimize these nanostructures for faster communication. These short DNA molecules, roughly 10 to 20 bp long and tethered to a DNA origami platform through a 3-nucleotide stretch of ssDNA (Fig. 3a), transport a particular strand of DNA along neighboring acrobats through strand-displacement reactions [29] initiated at the non-tethered end of the donor molecule. The stiffness of the foothold introduces a bias in the positions sampled by this free end, which may be approximated by means of a harmonic potential (Fig. 3b). Due to their short length (much smaller than persistence length of dsDNA), these molecules are relatively rigid and sample conformations on a hemispherical surface (Fig. 3c). The binding-time expressions derived here for harmonically restrained two-dimensional walkers should then model well the kinetics of strand exchange between a pair of molecules which communicate through their non-tethered ends, a process that can be idealized as a reaction between these ends diffusing in separated but identical two-dimensional quadratic energy landscapes, or between two molecules which communicate end-to-foothold, a process that can be idealized as a reaction between a non-tethered end diffusing in a two-dimensional quadratic energy landscape and a fixed target.

Several parameters of the model need to be determined before our theory can be applied to this system. The standard deviation σ of the displacement of the free end of an acrobat around its mean position (which then yields the stiffness of the harmonic potential via $k = 1/\beta\sigma^2$) and its intrinsic diffusion coefficient D are both obtained from coarse-grained simulations [30, 31], as shown in Sec. 4 of [28]. Such accurate modeling of the foothold via simulations was required because the interactions between the surface and the tethered end of the acrobat can dramatically influence the dynamics of the non-tethered end [32].

The remaining parameter, κ, can be roughly estimated through flux balance from the bimolecular rate constant k_{on} of the displacement reaction in solution. For a local concentration of invading strands c_0 (approximated by the bulk one), the total flux J of these strands (in units of molecules per unit time) across a surface of radius ϵ is given by $J = \kappa \int_{|\mathbf{r}|=\epsilon} c_0 ds$, which can be written as $4\pi\epsilon^2 c_0 \kappa$. As strand displacement proceeds when the molecules are within a distance ϵ, removing molecules at a frequency of $k_{on}c_0$, the total flux is given by $J = (k_{on}c_0)(\frac{4}{3}\pi\epsilon^3 c_0)$ and, therefore, $\kappa = k_{on}c_0\epsilon/3$. Using the phenomenological model of reversible toehold exchange derived by Zhang and Winfree [29, 33], $k_{on} = k_f \times p_{bm|toe}$, where $k_f \approx 3\times10^6$ M^{-1}s^{-1} is their fitted rate constant for toehold hybridization and $p_{bm|toe}$ is the probability of a successful completion of branch migration once this process has been initiated (see Appendix A.I). It is then easily shown that the communication between DNA walkers is severely reaction limited as $\lambda^* = 2D\sqrt{\beta k}/\kappa \gg 1$ under the experimental conditions of interest ($c_0 = 10^{-4}$ M, $\sigma \gg 1$ nm, $\epsilon \ll a \sim 7$ nm and $p_{bm|toe} < 1$ [22]).

Using Eq. 10b for the reaction-limited binding scenario, a linear communication speed may be defined as $a/\tau_\kappa \sim \frac{\kappa}{2}\sqrt{a\epsilon\beta k/\pi}e^{-\frac{\beta k}{4}(a-\epsilon)^2}$ for small values of ϵ^* and large values of a^*. This suggests an optimal spacing between walkers of the order of the standard deviation of their motion (fluctuations) $a \approx \epsilon/2 + \sqrt{\epsilon^2/4 + 1/\beta k} \approx \epsilon/2 + \sigma$ for fixed σ (obtained via $\partial(a/\tau_\kappa)/\partial\epsilon|_\sigma = 0$), or an optimal fluctuation standard deviation $\sigma \approx (a-\epsilon)/\sqrt{2}$ for a fixed a (obtained via $\partial(a/\tau_\kappa)/\partial\sigma|_a = 0$), suggesting an intrinsic match between walker length and foothold spacing which maximizes communication speed. While the foothold spacing on DNA origami platforms has to be a multiple of a turn of the helix (∼3.5 nm), there is more control over the fluctuation size σ, which may be tuned by changing the length of the DNA walkers (Fig. 3d). In Fig. 3e we evaluate our predicted communication speeds a/τ under experimental conditions for the scenario of two walkers binding with constant reactivity κ through their non-tethered ends (solid blue -dark-line) along with three other scenarios introduced further below. While branch migration models alone provide results of the same order of magnitude as experiments [22], they predict an inverse relation between communication speed and length of the walker, contrary to experimental findings of an optimal length which maximizes communication speed. In contrast, such a maximum in communication speed is correctly captured by our model (Eq. 10b), which shows a minimum in the binding time

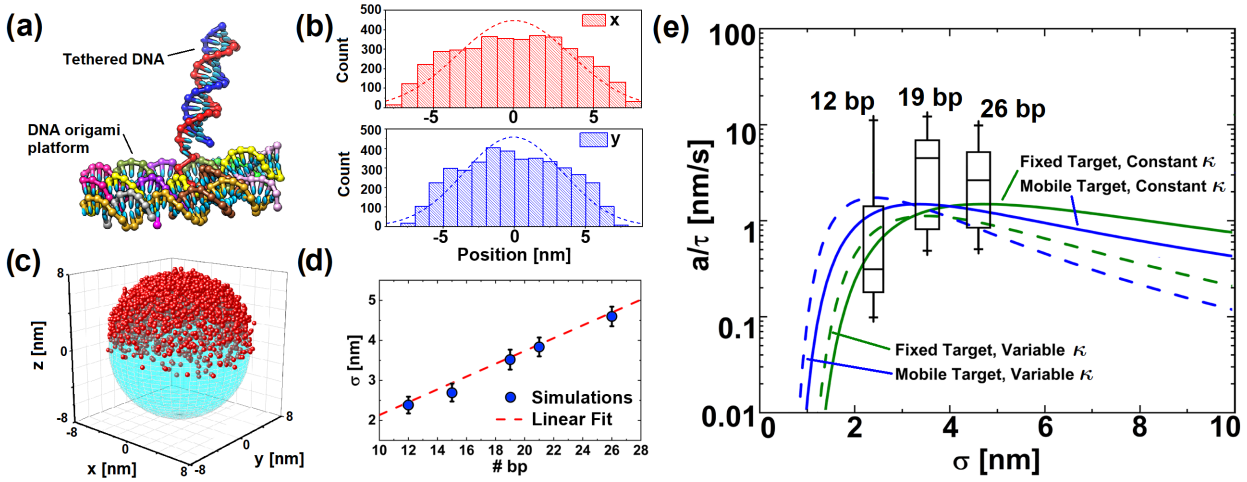

FIG. 3. Application to DNA acrobats: (a) 19-bp long DNA walker simulated through oxDNA. (b) Histogram of the position of the free end of this walker with respect to its foothold along two orthonormal axes parallel to the DNA origami platform. Fitting to a normal distribution (dashed lines) yields a standard deviation of $\sigma = 3.5$ nm. (c) Positions sampled by the free end follow a roughly hemispherical surface. (d) Standard deviation of the motion of free ends for walkers of different lengths (symbols). Dashed line denotes linear fit to data. (e) Comparison of theoretical and experimental communication speeds for $a = 7$ nm, $\epsilon = 2$ nm (roughly the diameter of a dsDNA molecule) and different experimentally tested dsDNA lengths. Blue (dark) and green (light) lines correspond to τ_κ for end-to-end and end-to-foothold communication scenarios. For each case, we examined length-dependent (dashed) and length-averaged (solid) reactivity κ.

τ_κ (Fig. 2d) with respect to the stiffness of the confining potential (directly related to the walker length, as shown in Fig. 3d). In fact, the location of this maximum ($\sigma = (a-\epsilon)/\sqrt{2} \approx 3.5$ nm corresponding to a 19 bp walker) coincides with experimental findings.

While this model reproduces well the experimental results, the probability of a successful completion of branch migration, and thereby κ, generally decreases with the length of the walker (see Appendix A.I). Also, strands are typically exchanged across walkers in an end-to-foothold rather than an end-to-end manner [22]. A model that incorporates both these effects, that is, a confined two-dimensional walker binding to a fixed target with variable reactivity κ, captures equally well the maximum and its location in the communication speed versus σ plot (dashed green -light- line, Fig. 3e). Interestingly, employing a length-dependent reactivity in the two-walker scenario (dashed blue -dark- line) and a length-independent reactivity in the one-walker scenario (solid green -light- line) shifts the position of the maximum towards shorter and longer walker lengths, respectively. The derivation of binding times for these additional scenarios are provided in Appendix B.

IV. CONCLUSIONS

In this work, we derived analytical expressions for the mean binding time of two walkers geometrically confined by means of harmonic potentials, both for one and two dimensional systems. These expressions were tested against a recently proposed Brownian dynamics algorithm for the estimation of MFPTs, and were shown to be in excellent agreement for different parameter regimes. While the analytical expressions derived here have been applied in the context of DNA nanotechnology, they open up avenues for understanding, predicting, and optimizing the binding or reaction kinetics of molecular systems of diverse nature under soft confinement, a scenario that is increasingly being encountered with the development of field- and chemistry-based approaches for controlling motion of nanoscopic and colloidal moieties.

ACKNOWLEDGMENTS

The authors acknowledge financial support from the National Science Foundation (Grant No. CMMI-1921955) and the Department of Energy (Grant No. DE-SC0020996), Wolfgang Pfeifer for providing the design file of the DNA origami platform used in this work, and the Texas Advanced Computing Center (TACC) at The University of Texas at Austin for providing HPC resources for carrying out the simulations presented in this work.

Appendix A. Branch Migration Probability and Length Dependence

A.I. Model for Toehold-Mediated Strand Displacement Reactions

Using the phenomenological model of reversible toehold exchange derived by Zhang and Winfree [29, 33], the bimolecular rate constant k_{on} can be written as $k_{on} = k_f \times p_{bm|toe}$, where k_f is their fitted rate constant for toehold hybridization, and $p_{bm|toe}$ is the probability of a successful completion of branch migration once this process has been initiated. This probability may be estimated through

$$p_{bm|toe} \approx \frac{k_b}{k_{rev} + k_b}, \tag{A.1}$$

where

$$k_{rev} \approx \frac{2k_f}{b-1} e^{-|\Delta G^o|/RT} \tag{A.2}$$

is the calculated unimolecular rate constant for toehold dissociation with $|\Delta G^o|$ the absolute free energy of binding between the toehold and its complement, $b-1$ is the number of bases left to displace after the first base has been displaced, and

$$k_b \approx \frac{400\ \mathrm{M^{-1}s^{-1}}}{(b-1)^2} \tag{A.3}$$

is their fitted rate constant for crossing the "half-way point" of branch migration. From the literature, $k_f = 3 \times 10^6\ \mathrm{M^{-1}s^{-1}}$ and $\Delta G^0 \approx -5.3$ kcal/mol for the toehold used in the experiments (AATGAG, whose energy we approximate to the energy of a weak toehold of length 6 [29]). While b is an integer number, we consider a continuum approximation $b = f(\sigma)$, where f is the inverse of the fitting function which relates the standard deviation σ with the length of the walker [28]. With these values, we get $p_{bm|toe} = 0.044$, 0.028 and 0.02 for branch migrations involving 12, 19 and 26 bases, respectively, and therefore we used $p_{bm|toe} = 0.03$ as our length-independent probability.

A.II. Effect of Length-Dependence on the Location of the Maxima

Note that the length-dependence of κ shifts the location of the maxima. For two moving walkers which bind in a 2D landscape (and small values of ϵ^* / large values of a^*),

$$\frac{a}{\tau_\kappa} \sim \frac{\kappa}{2}\sqrt{\frac{a\epsilon\beta k}{\pi}} e^{-\frac{\beta k}{4}(a-\epsilon)^2} \approx \frac{k_{on}c_0\epsilon}{6}\sqrt{\frac{a\epsilon\beta k}{\pi}} \frac{e^{-\frac{\beta k}{4}(a-\epsilon)^2}}{1+(b-1)\frac{k_{rev}}{k_b}}. \tag{A.1}$$

Writing $\sigma^2 = 1/\beta k$, $b = f(\sigma)$,

$$\frac{a}{\tau_\kappa} \sim \frac{k_{bind}c_0\epsilon}{6}\sqrt{\frac{a\epsilon}{\pi\sigma^2}} \frac{e^{-\frac{1}{4\sigma^2}(a-\epsilon)^2}}{1+[f(\sigma)-1]\frac{k_{rev}}{k_b}}, \tag{A.2}$$

and taking the derivative of this expression with respect to σ, we can find the values of σ which maximize speed by solving $\frac{\partial}{\partial\sigma}(\frac{a}{\tau_\kappa}) = 0$,

$$[(a-\epsilon)^2 - 2\sigma^2](1+[f(\sigma)-1]\tfrac{k_{rev}}{k_b}) - 2\frac{k_{rev}}{k_b}\frac{\partial f(\sigma)}{\partial\sigma}\sigma^3 = 0 \tag{A.3}$$

which yields the location specified in the main manuscript for $f(\sigma) = 1$, and shifts it an amount trivial to determine numerically for any other values of $f(\sigma)$.

Appendix B. Extension of our Methodology to Fixed Targets

B.I. One walker binding to a fixed target in 1D

Consider a single walker of diffusion coefficient D moving in one dimension around an attractive center located at $x = 0$. By modeling the attraction to this center through a harmonic potentials with second derivative k, the probability of finding this particle at a location x is given by

$$P(x) = \left(\frac{\beta k}{2\pi}\right) e^{-\frac{\beta k}{2}x^2}. \tag{B.1}$$

Measuring the distance of this walker to a fixed target placed at $x = a$, and writing $x = a + r$, the probability density for a distance r between the walker and the target is given by

$$Q(r) = \sqrt{\frac{2\beta k}{\pi}} \left(\frac{e^{-\frac{\beta k}{2}(a+r)^2}}{\mathrm{erfc}\left(\sqrt{\frac{\beta k}{2}}(\epsilon + a)\right)} \right) \tag{B.2}$$

and the reaction-limited MFPT is nothing more than $\tau_\kappa = 1/\kappa Q(\epsilon)$.

B.II. One walker binding to a fixed target in 2D

Consider a single walker of diffusion coefficient D moving in two dimensions around an attractive center located at $(x, y) = (0, 0)$. By modeling the attraction to this center through a harmonic potentials with second derivative k, the probability of finding this particle at a location (x, y) is given by

$$P(x) = \left(\frac{\beta k}{2\pi}\right)^2 e^{-\frac{\beta k}{2}(x^2+y^2)}. \tag{B.3}$$

Measuring the distance of this walker to a fixed target placed at $(x, y) = (a, 0)$, and writing $x = a + rcos(\theta)$, $y = rsin(\theta)$ analogous to the two walker case we can show that the probability density for a distance r between the walker and the target is given by

$$Q(r) = \frac{re^{-\frac{\beta k}{2}r^2} I_0\left(\beta kar\right)}{\int_{\epsilon}^{+\infty} re^{-\frac{\beta k}{2}r^2} I_0\left(\beta kar\right) dr} \tag{B.4}$$

and the reaction-limited MFPT is nothing more than $\tau_\kappa = 1/\kappa Q(\epsilon)$.

* Corresponding Authors:
ss1212@duke.edu, gaurav.arya@duke.edu

[1] S. Redner, *A guide to first-passage processes* (Cambridge University Press, 2001).
[2] H. Berg, Randoms walks in biology: New and expanded edition (1992).
[3] C. W. Gardiner *et al.*, *Handbook of stochastic methods*, Vol. 3 (springer Berlin, 1985).
[4] J. F. Douglas, Aspects and applications of the random walk (1995).
[5] K. Spendier and V. Kenkre, Analytic solutions for some reaction-diffusion scenarios, J. Phys. Chem. B **117**, 15639 (2013).
[6] D. Holcman and Z. Schuss, The narrow escape problem, Siam Rev. **56**, 213 (2014).
[7] A. E. Lindsay, A. J. Bernoff, and M. J. Ward, First passage statistics for the capture of a brownian particle by a structured spherical target with multiple surface traps, Multiscale Model. Sim. **15**, 74 (2017).
[8] K. Murthy and K. Kehr, Mean first-passage time of random walks on a random lattice, Phys. Rev. A **40**, 2082 (1989).
[9] S. Condamin, O. Bénichou, V. Tejedor, R. Voituriez, and J. Klafter, First-passage times in complex scale-invariant media, Nature **450**, 77 (2007).
[10] M. Gitterman, Mean first passage time for anomalous diffusion, Phys. Rev. E **62**, 6065 (2000).
[11] D. S. Grebenkov, First passage times for multiple particles with reversible target-binding kinetics, J. Chem. Phys. **147**, 134112 (2017).
[12] P. Jung, Periodically driven stochastic systems, Phys. Rep. **234**, 175 (1993).
[13] F. Le Vot, S. Yuste, E. Abad, and D. Grebenkov, First-encounter time of two diffusing particles in confinement, Phys. Rev. E **102**, 032118 (2020).
[14] M. v. Smoluchowski, Versuch einer mathematischen theorie der koagulationskinetik kolloider lösungen, Z. Phys. Chem. **92**, 129 (1918).
[15] V. Tejedor, M. Schad, O. Bénichou, R. Voituriez, and R. Metzler, Encounter distribution of two random walkers on a finite one-dimensional interval, J. Phys. A - Math. Theor. **44**, 395005 (2011).
[16] K. C. Neuman and A. Nagy, Single-molecule force spectroscopy: optical tweezers, magnetic tweezers and atomic force microscopy, Nat. Methods **5**, 491 (2008).
[17] J. F. Beausang, C. Zurla, L. Finzi, L. Sullivan, and P. C. Nelson, Elementary simulation of tethered brownian motion, Am. J. Phys. **75**, 520 (2007).
[18] S. Bell and E. M. Terentjev, Kinetics of tethered ligands binding to a surface receptor, Macromolecules **50**, 8810 (2017).
[19] S. Sugaya and V. Kenkre, Analysis of transmission of infection in epidemics: Confined random walkers in dimensions higher than one, B. of Math. Biol. **80**, 3106 (2018).
[20] A. Szabo, K. Schulten, and Z. Schulten, First passage time approach to diffusion controlled reactions, J. Chem. Phys. **72**, 4350 (1980).
[21] A. B. Adib, Algorithms for brownian first-passage-time estimation, Phys. Rev. E **80**, 036706 (2009).
[22] J. Li, A. Johnson-Buck, Y. R. Yang, W. M. Shih, H. Yan, and N. G. Walter, Exploring the speed limit of toehold exchange with a cartwheeling DNA acrobat, Nat. Nanotechnol. **13**, 723 (2018).
[23] J. S. Lucas, Y. Zhang, O. K. Dudko, and C. Murre, 3D trajectories adopted by coding and regulatory DNA elements: first-passage times for genomic interactions, Cell **158**, 339 (2014).
[24] A. Schena, R. Griss, and K. Johnsson, Modulating protein activity using tethered ligands with mutually exclusive binding sites, Nature communications **6**, 1 (2015).
[25] E. W. Visser, J. Yan, L. J. van IJzendoorn, and M. W. Prins, Continuous biomarker monitoring by particle mobility sensing with single molecule resolution, Nature communications **9**, 1 (2018).
[26] R. Erban and S. J. Chapman, Reactive boundary conditions for stochastic simulations of reaction–diffusion processes, Phys. Biol. **4**, 16 (2007).
[27] S. Lawley and J. Madrid, First passage time distribution of multiple impatient particles with reversible binding, J. Chem. Phys. **150**, 214113 (2019).
[28] See *Supplementary Materials* at [URL will be inserted by publisher] for explicit derivations and simulation details.
[29] D. Y. Zhang and E. Winfree, Control of DNA strand displacement kinetics using toehold exchange, J. Am. Chem. Soc. **131**, 17303 (2009).
[30] P. Šulc, F. Romano, T. E. Ouldridge, L. Rovigatti, J. P. K. Doye, and A. A. Louis, Sequence-dependent thermodynamics of a coarse-grained DNA model, J. Chem. Phys. **137**, 135101 (2012).
[31] Z. Shi, C. E. Castro, and G. Arya, Conformational dynamics of mechanically compliant DNA nanostructures from coarse-grained molecular dynamics simulations, ACS Nano **11**, 4617 (2017).
[32] E. Farjami, R. Campos, and E. E. Ferapontova, Effect of the DNA end of tethering to electrodes on electron transfer in methylene blue-labeled DNA duplexes, Langmuir **28**, 16218 (2012).
[33] N. Srinivas, T. E. Ouldridge, P. Šulc, J. M. Schaeffer, B. Yurke, A. A. Louis, J. P. Doye, and E. Winfree, On the biophysics and kinetics of toehold-mediated DNA strand displacement, Nucleic Acids Res. **41**, 10641 (2013).